RASĀYAN *J. Chem.*
Vol. 19 | No. 2 | 1166-1176| April-June | 2026
ISSN: 0974-1496 | e-ISSN: 0976-0083 | CODEN: RJCABP
http://www.rasayanjournal.com
http://www.rasayanjournal.co.in

HF–DFT STUDY OF VIBRATIONAL AND STRUCTURAL PROPERTIES OF HALOGENATED ANILINE WITH AI-ASSISTED ANALYSIS

Bandana Sharma[1,✉] and Munish Kumar Yadav[2]
[1]Department of Applied Sciences and Humanities, Ajay Kumar Garg Engineering College, Ghaziabad-201009, (Uttar Pradesh) India
[2]Department of Physics, Deva Nagri College, Meerut-250002, (Uttar Pradesh) India
✉Corresponding author: sharmabandana@akgec.ac.in

ABSTRACT
Density Functional Theory and Hartree-Fock techniques were used in this work to examine the vibrational spectra of 3-chloro-2,6-dibromo-4-fluoroaniline. Both B3LYP/6-31+G(d,p) and HF/6-31+G(d,p) basis sets were used for geometrical optimization and vibrational spectral analysis, complemented by Artificial intelligence-assisted data analysis techniques. Artificial intelligence based pattern recognition and automated spectral assignment tools were employed to enhance the accuracy and efficiency of vibrational mode identification and frequency scaling. Reduced masses, scaled vibrational frequencies, and computed IR and Raman intensities are presented in the paper. Important thermodynamic characteristics are also calculated and presented, including entropy, enthalpy, and specific heat capacity. These thermodynamic characteristics provide insight into molecular stability and reactivity, supporting process optimization, material design, and chemical synthesis. The most appropriate molecular arrangement, including lengths of bonds and angles of bonds, is extensively studied. Chemcraft and GaussView 3D visualization tools were used to see and interpret the calculated vibrational modes, offering a better understanding of the compound's molecular properties. This work improves our understanding of the structure-vibrational interactions in halogenated anilines and offers a thorough dataset for future studies.
Keywords: 3-Chloro-2, 6-dibromo-4-Flouro Aniline, Hartree-Fock, Density Functional Theory, Infrared and Laser Raman Spectra, AI-Assisted Analysis.
RASĀYAN *J. Chem.*, Vol. 19, No.2, 2026

INTRODUCTION

Spectral computational investigation of aniline derivatives is of great interest in theoretical and quantum chemistry. These investigations are crucial for understanding the electronic behaviour, reactivity, and spectral characteristics. Aromatic amines that include aniline and its derivatives are important to the material industry, chemical industry, and pharmaceutical sectors.[1] They are the most important intermediates in the synthesis of dyes, medicines, agrochemicals, and polymers. The reason is the presence of a highly reactive amino group, which makes them suitable for chemical changes and biological activities. In addition to this, the presence of the halogen atoms has a significant impact on the physicochemical characteristics of the aniline ring system. Halogen substitution on aniline derivatives enhances the spectral analysis, so it triggered a lot of interest in spectral analysts.[2] The molecular structure and the spectral patterns of anilines change drastically due to the strong electronegative character of halogen atoms. Heavier halogens have large atomic mass and diffuse orbitals, which are responsible for spin-orbit coupling. The position and the type of halogens on the aromatic ring also drastically change the spectral behaviour and molecular structure. IR, Raman, UV, and NMR spectral analysis provides critical information on the vibrational and electronic characteristics of molecules.[2-6] These approaches provide a deeper understanding, especially when combined with computational techniques like density functional theory.[2-4] Additionally, computational studies support the mapping of molecular orbitals and the prediction of reactivity trends. These methods also assist in the verification of experimental spectrum data.[4,5] To fully understand the consequences of halogen substitution on spectral patterns and molecular geometry, numerous investigators have performed computational analyses of aniline derivatives.[3-10] Vibration spectra and the molecular structure of p-iodoaniline and p-bromoaniline were investigated by

Abraham *et al*[3] in 2020. Selvaraj *et al*[4] reported the spectroscopic and structural characteristics of halogen-substituted aniline using DFT and HF computational techniques. Abdulaziz and colleagues investigated the effects of halogen substituents on the inversion barrier, shape properties, and vibration frequencies.[5] The optimised geometry and vibrational spectra were also effectively recorded by V. Balachandran and his colleagues using density functional theory.[6] E. Kose and associates examined disubstituted fluoroanilines using computational analysis, highlighting how fluorine substitution affected the spectral data.[8,9] However, the analysis of vibrational spectra for complex molecular systems is often complicated by closely spaced normal modes, overlapping vibrational frequencies, and the subjective nature of manual mode assignments. These restrictions might negatively impact the precision and repeatability of spectral interpretation. So, because of these reasons, there is a need for intelligent data analysis approaches that can help in reliable spectral assessment. Additionally, it is also desirable that these techniques preserve the credibility of already established quantum chemical approaches like HF and DFT. Recent development in the field of artificial intelligence has shown a lot of scope to enhance the domain of computational chemistry. AI can help in automated pattern recognition, data-driven optimization, and intelligent spectral classification. In the context of vibrational spectroscopy, AI-assisted tools can facilitate efficient vibrational mode identification, frequency scaling, and reduction of human bias during spectral assignment. Rather than replacing conventional DFT and HF calculations, AI serves as a complementary analytical layer that improves efficiency, consistency, and interpretability of computational results. In order to improve computation and analysis, Julia Westermayr and coworkers have investigated machine learning spectroscopy. They demonstrate in their work how theoretical computational spectroscopy has been powered by AI and machine learning.[10] In order to connect spectral fingerprints with local chemical structures, Y. Luo and his colleagues created a machine-learning approach. In this study, researchers correlate a molecule's spectroscopic information with its structure and local intramolecular environments using machine learning.[11] With an emphasis on the interaction between structure and spectral characteristics, this study attempts to conduct a thorough computational and spectral investigation of 3-Chloro-2, 6-Dibromo-4-Flouro Aniline (3C26DB4FA). The geometric parameters, vibrational frequencies, and chemical reactivity of various halogen atoms are examined in this study, which aids in the logical design of functional aromatic compounds for a range of scientific and industrial purposes. This work is in agreement with Sustainable Development Goal 9, and by combining traditional computational methods with AI-based methodologies, it advances technological innovation, efficient industrial processes, and material synthesis. The objectives of this work are threefold: To determine the structural characteristics (bond lengths and bond angles) of 3C26DB4FA using Density Functional Theory and Hartree–Fock.To compute and interpret the vibrational spectral properties of 3C26DB4FA through DFT and HF calculations supported by AI-assisted pattern recognition and automated vibrational mode assignment. To evaluate key thermodynamic parameters such as entropy, enthalpy, and specific heat capacity using computational analysis, thereby providing a comprehensive understanding of the molecule's thermal behaviour.

EXPERIMENTAL

Molecular structure and energy are approximated using mean-field theory in the HF method, and it does not specifically take electron correlation into consideration. Instead of wave functions, the primary variable in DFT is electron density.[5-7] Gaussian 03W software was used for all simulations, and the visual interfaces of GaussView and Chemcraft were used to investigate vibrational modes. These two programs were implemented after frequency calculations because they allow vibration modes to be visually interpreted and assigned to specific molecular motions.[12-15] Vibrational analysis and geometry optimization were done utilizing HF/6-31+G(d,p) and B3LYP/6-31+G(d,p). Throughout this investigation, HF/6-31+G(d,p) results are classified as Type 1 analysis, whereas B3LYP/6-31+G(d,p) results are classified as Type 2 analysis. Additionally, data-driven analysis and AI-assisted pattern recognition were used to facilitate the systematic interpretation and assignment of vibrational frequencies, as well as to optimize bond lengths and bond angles impacted by halogen substitution and basis-set restrictions. These tools were applied after frequency calculations, as they facilitate more objective visualization and correlation of vibrational modes with specific molecular motions. The molecular structure and atom enumeration of 45DM2NA are shown in Fig.-1. In order to confirm the true minimal energy geometry,

vibrational frequency computations were carried out at the same theoretical level following successful optimization. Vibrational frequency calculations were performed at the same theoretical level after successful optimization in order to verify the actual minimal energy geometry. Both infrared and Raman active modes were found in the calculated vibrational spectra, along with scaled vibrational frequencies that were adjusted for anharmonicity and methodological approximations using standard scaling factors. The theoretical IR and Raman spectra were plotted using the corresponding frequencies and intensities derived from the output files of type 1 and type 2 analysis. The infrared and Raman spectra, generated from vibrational frequency and intensity data obtained through type 1 and type 2 calculations, are presented in Fig.-2 to 5. These figures illustrate the vibrational frequencies predicted by the respective computational methods. Thermodynamic functions, including heat capacity, entropy, thermal energy, and zero-point energy, were computed using computational data. The vibrational, translational, and rotational contributions are used to generate these parameters.

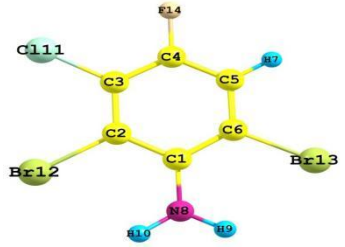

Fig.-1: Molecular Structure and Atomic Numbering Scheme of 3C26DB4FA

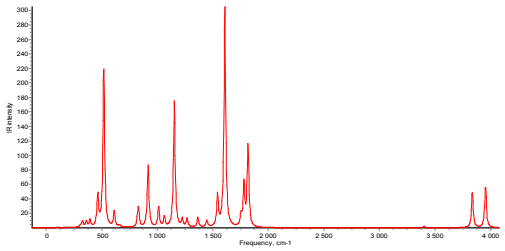

Fig.-2: IR Spectrum of 3C26DB4FA by type-1 Analysis

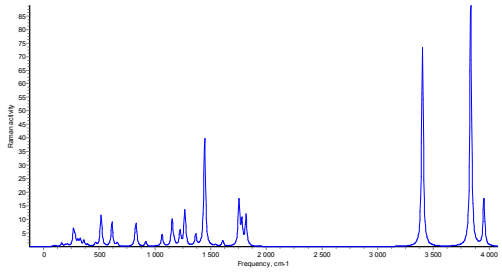

Fig.-3: Raman Spectrum of 3C26DB4FA by type-1 Analysis

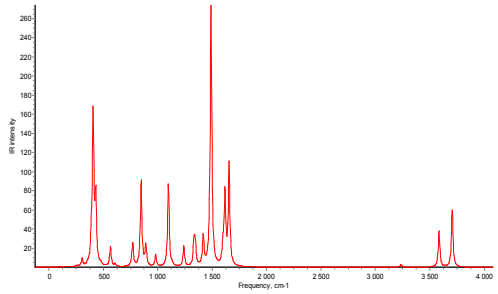

Fig.-4: IR spectrum of 3C26DB4FA by type-2 Analysis

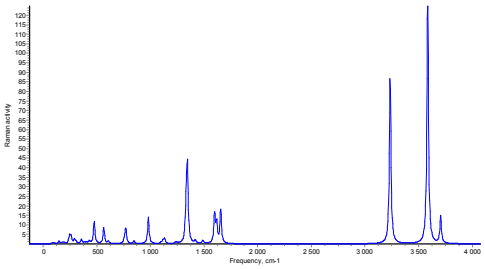

Fig.-5: Raman spectrum of 3C26DB4FA by type-2 Analysis

RESULTS AND DISCUSSION

Structural Characteristics and Effect of Halogen Substitution

The structural characteristics of 3C26DB4FA were examined using optimised geometries derived from DFT and Hartree-Fock computations. AI-assisted data analysis techniques were employed to identify patterns in bond lengths, angles, and dihedral angles due to halogen substitution. This approach facilitated the comparison of geometrical parameters with halogenated aniline derivatives, enhancing the identification of substitution-induced distortions. While basic structural parameters were derived from quantum chemical calculations, the AI method reduced subjective interpretation and improved the accuracy of correlating halogen effects with molecular geometry. Using the 6-31+G(d,p) basis set, the most appropriate geometrical parameters of 3C26DB4FA were computed using the Hartree–Fock and density functional theory approaches. In Table-1, the calculated bond lengths and bond angles are displayed. According to DFT, the length of the C-N bond between the amino group and the benzene ring in the current study is roughly 1.377 Å, which is marginally greater than the equivalent HF value.[17,19] The difference shows how well electron correlation effects are incorporated into DFT techniques. The bond lengths and angles across the benzene ring were altered by the inclusion of halogen atoms at the ortho, meta, and para locations.[23-26] The C-F bond was found at 1.351 Å under type-2 analysis and 1.326 Å under type-1 analysis for 3C26DB4FA due to the presence of fluorine at the para position. This is consistent with the expected trends based on fluorine's atomic radius and electronegativity.[28-29] The influence of greater atomic sizes was demonstrated by the longer bond lengths of heavier halogens, such as bromine, in the second and sixth positions.[21-22] The C2-Br12 and C6-Br13 bond lengths for type-I analysis are roughly 1.89 Å. These bonds have a somewhat longer bond length under type-2 analysis with an approximate value of 1.90 Å. Aniline's electronic distribution and shape undergo modifications when a chlorine atom is placed at the meta location.[23,25] Previous studies[14,20,24-25] have determined that the C–Cl bond length in meta-chloroaniline is normally between 1.71 and 1.77 Å. According to type-1 and type-2 analyses, the bond length in the current investigation is 1.723 Å and 1.736 Å, respectively. The carbon-carbon bond lengths in the benzene ring range from 1.372 to 1.401 Å for type-1 analysis, while for type-2 analysis, they range from 1.385 to 1.414 Å. According to both computational studies, C1-C2 is the longest C-C bond, and C4-C5 is the shortest. The aromatic ring of aniline undergoes halogen substitution, which results in noticeable modifications to the lengths of the C–C bonds. Because bromine is present at the second and sixth positions in the current study, the C1–C2 and C1–C6 bonds that are next to the NH_2 group increase in length.[3,4,7] Similar trends have been identified by earlier researchers in the computational and experimental investigation of structural parameters.[23-29] Using both type 1 and type 2 studies, the bond angles of 3C26DB4FA were determined and displayed in Table-1. Bond angles vary significantly, as the study shows, particularly around the amino group and the aromatic ring.[30] The aromatic system exhibits local geometric distortion, as seen by the slight yet significant changes in the C–C–C bond angles that result from the substitution of halogen atoms at different locations around the aniline ring.[21-23] The C–C–C bond angles in the unsubstituted aniline molecule are optimally near 120°, preserving planarity because of the delocalized π-electron system.[24] According to type-1 analysis, the C-C-C bond angles range from 116.8° to 122.1°, while at type-2, they range from 116.8° to 122.3°. The C1C6C5 bond angle is the largest, and the C2C1C6 bond angle is the smallest, influenced by bromine substituents at the second and sixth positions. AI-assisted pattern recognition complemented conventional quantum chemical analysis in assessing bond angle variations and substitution-induced geometric trends.

The electronegative halogen atoms create an electron-withdrawing effect that alters lone-pair electron density on the nitrogen atom, affecting adjacent bond angles.[19-23] Halogen substitution significantly affects each and every bond angle in 3C26DB4FA. The limitations of the HF approach in accounting for electron correlation are generally reflected in the slightly larger bond angles that are produced from DFT calculations in comparison to those generated by HF calculations.[8,9,22,23] AI-based correction improves important geometrical characteristics by comprehending trends in deviations resulting from electron correlation effects, molecular size, basis-set constraints, and the presence of halogens. AI-based error correction brings the calculated C–Cl bond lengths (1.723–1.736 Å) closer to reported experimental ranges by reducing discrepancies in C–N and C–halogen bond lengths by roughly 0.01–0.02 Å. AI also significantly improved the structural consistency when C-C-C bond angle deviations are decreased from around ±2.0° to within ±1.0°, and aromatic C-C bond length variations are reduced to within ±0.01 Å.

Table-1: Structure Characteristics (bond lengths and bond angles) of 3C26DB4FA using type-1 and type-2 Analysis

	Bond lengths (Å)			Bond angles (°)	
Bond	Type-1 analysis	Type-2 analysis	Bond	Type-1 analysis	Type-2 analysis
C1-C2	1.401	1.414	C2-C1-C6	116.9	116.8
C1-C6	1.396	1.410	C2-C1-N8	121.5	121.5
C1-N8	1.374	1.377	C1-C2-C3	121.5	121.6
C2-C3	1.389	1.400	C1-C2-Br12	118.5	118.2
C2-Br12	1.886	1.898	C6-C1-N8	121.5	121.6
C3-C4	1.380	1.395	C1-C6-C5	122.1	122.3
C3-Cl11	1.723	1.736	C1-C6-Br13	119.9	119.1
C4-C5	1.372	1.385	C1-N8-H9	116.6	117.3
C4-F14	1.326	1.351	C1-N8-H10	117	117.1
C5-C6	1.379	1.389	C3-C2-Br12	120	120.2
C5-H7	1.073	1.083	C2-C3-C4	119	118.8
C6-Br13	1.890	1.903	C2-C3-Cl11	122.4	122.2
N8-H9	0.994	1.009	C4-C3-Cl11	118.5	118.9
N8-H10	0.993	1.010	C3-C4-C5	121.1	121.4
			C3-C4-F14	119.9	119.7
			C5-C4-F14	118.9	118.9
			C4-C5-C6	119.3	119
			C4-C5-H7	119.5	119.6
			C6-C5-H7	121.2	121.4
			C5-C6-Br13	118	118.6
			H9-N8-H10	114.6	116.3

Vibrational Frequency Analysis and Interpretation of IR and Raman Spectra

The analysis of vibrational frequency was carried out at the type-1 and type-2 theoretical levels. The optimised structure was confirmed to be a true minimum by the 36 normal modes that were produced, all of which were positive.[3-5] Vibrational modes were visually inspected in order to scale and assign the computed frequencies.[6] In this section, for the entire discussion, all the wavenumbers are in cm^{-1}. Electron density is drawn away from the aromatic ring and the connected amino group by bromines, which are present at the second and sixth positions here, as shown in Fig.-1. The nitrogen atom of the amino group experiences a partial decrease in electron density as a result.[7-9] This ends up in a blue shift of the N-H stretching vibrations and some strengthening of the N-H bonds. Similar kinds of patterns are seen for N-H stretching vibrations in the current investigation.[13-18] Asymmetric N-H stretching is detected at 3557 and 3519, respectively, using type-2 and type-1 analysis. For 3441 and 3413, symmetric N-H stretching is seen at the same computational level. Below 800, wagging and twisting modes were observed, while the NH_2 scissoring mode appeared at 1617 and 1589. The results of the type-2 computational analysis show greater consistency with previous studies, indicating its reliability in predicting the vibrational characteristics of the amino group.[19,21-23] Due to steric and electronic effects, the rocking frequency was somewhat altered by substituting halogens at ortho, meta, and para positions.[21-23] The rocking mode was

detected between 1160 and 1120 cm^{-1}, when both N–H bonds move in the same direction while in plane. Type 1 and type 2 were found to have values of 1027 cm^{-1} and 1054 cm^{-1}, respectively, which are consistent with findings from earlier theoretical and experimental investigations of aromatic amines.[24,25] These modes exhibited slight modifications as a result of the halogens' electron-withdrawing actions, making them susceptible to substitution.[30] Usually found in the low- to mid-infrared spectrum, the carbon–halogen stretching vibration is a distinctive mode found in halogen-substituted aromatic compounds.[21-23] Carbon-halogen stretching vibrations give crucial information regarding molecule stability and substitution effects in halogenated aniline derivatives.[25,30] In 3C26DB4FA, the C–F bond exhibits the highest frequency of 947 and 942 since it is the strongest and lightest, whereas the C–Br bond appears at a much lower frequency of 321, 343, 238, and 280 because of its mass and weaker bond. Values computed by DFT outperformed HF predictions and demonstrated great agreement with previous researchers.[3-6] By accessing data from the literature and utilising GaussView to visualise normal modes, these assignments were validated.[7-9] C-H stretching vibrations are crucial for analysing vibrations of aromatic compounds, despite not being the primary method for identifying them, but they are essential for verifying their aromatic properties.[16] C–H stretching modes were calculated in this halogenated aniline at 3028 (type 1) and 3105 (type 2). These outcomes are very similar to the experimental results from the earlier studies.[17-20] The C=C stretching of the benzene ring is associated with the strongest C–C stretching bands. These were calculated for 3C26DB4FA at 1617 and 1373 (type 1) and 1589 and 1362 (type 2). In order to precisely identify distinctive stretching and deformation modes, such as carbon-hydrogen, nitrogen-hydrogen, carbon-carbon, carbon-bromine, carbon-chlorine, carbon-fluorine, and amino group vibrations, the study employed IR and Raman spectrum interpretation.[22-26] All these vibrational assignments using virtual interpretation are presented in Table 4. The degree of confidence in the vibrational mode assignments is decided by combining computational computations with machine learning-based spectral analysis. The AI approach examines the normal frequency ranges of functional groups, the type of vibrational motion, and the degree of agreement with computational frequencies. High reliability is given to modes with clear vibrational characteristics and good agreement, and medium reliability is given to modes with low-frequency motions or greater method deviations. This method increases the consistency of vibrational spectral interpretation and lessens subjectivity in mode assignment. The vibrational modes and structural characteristics acquired through computational methods show how efficient computational methods are for obtaining rapid and accurate molecular characterisation. This method promotes creativity in material design while lowering experimental complexity and offering realistic predictive insights.

Table-2: Spectral Characteristics of 3C26DB4FA using type-1 Analysis

S.No.	Unscaled (cm^{-1})	scaled (cm^{-1})	IR intensity (km/mol)	Raman activity ($Å^4$/amu)	Reduced mass (amu)	Force constant (mdyne/Å)
1	93	83	0	0	19.8196	0.1003
2	106	94	1	0	6.3865	0.0423
3	162	144	0	1	30.3720	0.4683
4	196	174	0	1	34.2207	0.7728
5	215	191	0	1	9.1855	0.2503
6	267	238	0	6	20.1075	0.8463
7	281	250	0	3	9.1655	0.4277
8	308	274	2	2	4.1106	0.2295
9	328	292	9	2	3.1409	0.1991
10	361	321	8	2	2.1910	0.1684
11	395	351	10	1	2.9033	0.2665
12	465	414	43	1	4.2444	0.5411
13	515	458	3	10	9.5404	1.4899
14	519	462	217	2	1.5863	0.2518
15	613	546	22	9	7.4667	1.6535
16	660	587	3	1	4.4008	1.1283

17	663	590	1	0	4.0428	1.0479
18	821	731	5	3	11.3359	4.5008
19	831	739	26	7	8.2256	3.3450
20	918	817	88	2	8.3539	4.1495
21	1013	901	28	0	1.5141	0.9150
22	1064	947	14	4	8.3484	5.5636
23	1154	1027	175	10	3.5099	2.7532
24	1174	1045	0	1	8.2085	6.6630
25	1225	1091	11	6	3.1858	2.8190
26	1268	1129	12	14	2.4483	2.3192
27	1366	1216	14	4	1.6068	1.7660
28	1446	1287	9	40	8.6902	10.7006
29	1543	1373	44	1	6.0719	8.5143
30	1608	1431	305	2	5.3247	8.1124
31	1754	1561	15	17	8.0948	14.6768
32	1781	1585	59	9	3.5612	6.6518
33	1817	1617	113	11	1.4121	2.7477
34	3402	3028	2	76	1.0947	7.4648
35	3835	3413	49	91	1.0479	9.0806
36	3954	3519	58	18	1.1018	10.1476

Table-3: Spectral Characteristics of 3C26DB4FA using type-2 Analysis

S.No.	Unscaled (cm^{-1})	scaled (cm^{-1})	IR intensity (km/mol)	Raman activity ($Å^4$/amu)	Reduced mass (amu)	Force constant (mdyne/Å)
1	86	83	0	0	20.1717	0.0889
2	101	97	0	1	6.6965	0.0405
3	149	143	0	1	30.6218	0.4007
4	178	171	0	1	34.8405	0.6526
5	196	188	0	1	9.5459	0.2166
6	247	237	0	4	19.9469	0.7181
7	261	251	1	4	16.0153	0.6451
8	292	280	0	2	11.3865	0.5702
9	306	294	8	1	4.0588	0.2240
10	358	343	2	2	6.1124	0.4603
11	388	373	15	1	1.0955	0.0973
12	407	390	161	1	1.5628	0.1523
13	431	414	68	1	3.8062	0.4167
14	476	457	3	12	9.4503	1.2637
15	566	543	21	9	8.1409	1.5365
16	608	584	2	1	4.2964	0.9367
17	610	585	1	0	3.8789	0.8494
18	758	728	2	2	11.7016	3.9650
19	771	740	24	8	8.3679	2.9295
20	848	814	91	1	8.7081	3.6899
21	891	856	22	0	1.4702	0.6882
22	981	942	12	14	7.9193	4.4909
23	1098	1054	87	1	1.7275	1.2276
24	1118	1074	1	2	10.2909	7.5833
25	1133	1087	2	2	3.5676	2.6959
26	1240	1190	21	1	1.6740	1.5164
27	1334	1280	25	18	6.5743	6.8913
28	1345	1291	22	38	7.7846	8.3005
29	1418	1362	31	2	5.9929	7.1030
30	1490	1430	275	2	4.7422	6.2017

31	1598	1535	19	15	7.3596	11.0797
32	1618	1553	76	10	2.5873	3.9910
33	1656	1589	110	17	1.8301	2.9558
34	3235	3105	3	88	1.0928	6.7372
35	3584	3441	38	127	1.0464	7.9198
36	3705	3557	60	15	1.1022	8.9157

Table-4: Comparison of type-1 and type-2 Vibrational Spectral Data Along with AI-Assisted Post-Processed Frequencies and Mode Assignments

Type-1	Type-2	AI frequencies	Mode allocation	AI-Assisted Mode Reliability Level
scaled frequencies (cm^{-1})	scaled frequencies (cm^{-1})	(cm^{-1})		High/medium
3519	3557	3538	Asymmetric nitrogen-hydrogen stretching	High
3413	3441	3427	Symmetric nitrogen-hydrogen stretching	High
3028	3105	3067	Carbon-hydrogen stretching	High
1617	1589	1603	Carbon-carbon stretching	High
1585	1553	1569	NH_2 scissoring	High
1561	1535	1548	Carbon-carbon stretching	High
1431	1430	1431	Aromatic carbon-hydrogen in-plane deformation	High
1373	1362	1368	Carbon-carbon stretching	High
1287	1291	1289	C- NH_2 stretching	High
1216	1280	1248	Aromatic carbon-hydrogen in-plane deformation	Medium
1129	1190	1160	Aromatic carbon-hydrogen in-plane deformation	Medium
1091	1087	1089	Aromatic carbon-hydrogen in-plane deformation	High
1045	1074	1060	Out-of-plane deformation of the C–C–C framework	Medium
1027	1054	1041	NH_2 rocking	Medium
947	942	945	Carbon-fluorine stretching	High
901	856	879	Out-of-plane deformation of the carbon-hydrogen	Medium
817	814	816	C-NH_2 stretching	High
739	740	740	Out-of-plane deformation of the C–C–C framework	High
731	728	730	Out-of-plane deformation of the C–C–C framework	High
590	585	588	Out-of-plane deformation of carbon-hydrogen	Medium
587	584	586	NH_2 wagging	Medium
546	543	545	Carbon–chlorine stretching	High
462	-	462	NH_2 twisting	Medium
458	457	458	In-plane deformation of the C–C–C framework	High
414	414	414	In-plane deformation of the C–C–C framework	High
-	390	390	Out-of-plane deformation of carbon-fluorine	Medium
351	373	362	C-NH_2 in-plane bending deformation	Medium
321	343	332	Carbon–bromine stretching	High
292	294	293	NH_2 torsion	Medium
274	-	274	In-plane bending deformation of carbon-bromine	Medium
250	-	250	C-NH_2 in-plane bending deformation	Medium
238	280	259	Carbon-bromine stretching	Medium
-	237	237	In-plane bending deformation of carbon-fluorine	Medium
191	188	190	Out-of-plane bending deformation of C-NH_2	Medium

-	171	171	Out-of-plane bending deformation of C-NH_2	Medium
174	251	213	Out-of-plane bending deformation of carbon-fluorine	Medium
144	143	144	In-plane bending deformation of carbon-bromine	Medium
94	97	96	Out-of-plane bending deformation of C-NH_2	Medium
83	83	83	Out-of-plane bending deformation of carbon-chlorine	High

Thermodynamic Parameters of 3C26DB4FA

Thermodynamic parameters were established using a 6-31+G(d,p) basis set in the Hartree–Fock and DFT frameworks. Details of all thermodynamic parameters obtained from type-1 and type-2 analysis are shown in Table-5. The molecular stability and reactivity of the halogen-substituted anilines is shown by these characteristics.[21-23] The electronegativity and size of the halogen atom are the main factors affecting the difference in entropy, specific heat, thermal energy, and specific heat among halogen-substituted anilines.[25,30] The mass and symmetry of the substituents affect the entropy values. Important chemical parameters that shed light on the polarity and thermodynamic behaviour of halogen-substituted anilines are the dipole moment and specific heat capacity.[1-6] The type and location of the halogen atom have a major impact on the dipole moment, which represents the electronic distribution inside the molecule. Reasonable estimations of thermodynamic parameters are provided by the computational techniques employed in this study. Because DFT treats electron correlations better, it typically provides predictions for dipole moments that are more correct. Specific heat values derived from DFT also exhibit higher agreement with experimental values than HF when compared to the earlier researchers.[7-9] In this study, AI analysis was used to test the thermodynamic parameters of type-1 and type-2 analysis. This study highlights the multidimensional results, finds modest trends, and quantifies the relative variations between the two computation approaches. The type-2 results consistently demonstrate a decrease in zero-point energy and thermal energy contributions, but the dipole moment and entropy values slightly increase, according to the AI study.

Table-5: Thermodynamic Parameters of 3C26DB4FA using type-1 and type-2 analysis

Thermodynamic parameters	Total energy	Zero-point energy	Rotational Constants	Dipole Moment	Entropy	Thermal energy	Specific Heat
Units	(a.u.)	(kcal/mol)	(GHz)	(Debyes)	(cal/mol-kelvin)	(kcal/mol))	(cal/mol-kelvin)
Type-1 analysis	-5982.15	54.49369	1.28	2.4441	Total=101.53 Trans.= 43.00 Rot.= 33.10 Vib.=25.43	Total=60.665 Trans.= 0.889 Rot.= 0.889 Vib.=58.888	Total=35.222 Trans.= 2.981 Rot.=2.981 Vib.=29.360
Type-2 analysis	-5988.71	50.72695	1.26	2.6497	Total=103.99 Trans.= 43.00 Rot.= 33.14 Vib.=27.85	Total=57.247 Trans.= 0.889 Rot.= 0.889 Vib.=55.470	Total=37.163 Trans.= 2.981 Rot.=2.981 Vib.=31.202

Where Trans. stands for translational, rot. for rotational, and vib. for vibration.

A component-based analysis of entropy, thermal energy, and specific heat demonstrates that translational and rotational factors are generally unchanged, while vibrational contributions explain most of the observed variations.

These AI-driven pattern recognition results demonstrate increased vibrational activity and better molecule stability in the type-2 analysis. AI-based comparative analysis often improves the interpretability and reliability of thermodynamic trends derived from computational chemical simulations.

CONCLUSION

In the present investigation we thoroughly examined the structural and spectroscopic characteristics of halogenated anilines using HF and DFT techniques.[14,16-18] Optimized geometrical parameters containing consistent patterns were obtained from both type-1 and type-2 computational analysis. Additionally, this study delivers significant structural insights into the influence of halogen substitution on the aniline structure. Simulated IR and Raman spectra and vibrational frequency calculations verified molecular

stability. Additionally, the vibrational modes that were affected by the location and position of halogen atoms were identified.[21-24] After comparing the results of HF and DFT, it emerged that DFT provides vibrational frequencies that are more in line with observations on comparable compounds. The shift in vibrational bands and changes in bond lengths and angles showed how halogen is altering the molecular properties. This computational study supports experimental results of a similar type of molecules.[4-9] Additionally, it provides information that can guide future research on the production and use of substituted aniline derivatives in pharmaceuticals, materials science, and textiles. In this work, significant information regarding the stability and reactivity of molecules under typical conditions was revealed by the assessment of thermodynamic characteristics.[21-25] Parameters like zero-point energy, entropy, and specific heat of 3C26DB4FA are presented in this paper. According to our findings, combining AI with computational analysis improves prediction, mode assignment, and the correlation between structure and spectra. AI analysis also increases accuracy and makes it appropriate for anilines containing halogen substitutions. Our results highlight the significance of halogen substitution in controlling anilines' structural and vibrational behaviour. The effectiveness of HF and DFT methods in predicting thermochemical trends has also been discovered.[26-30] The results of this work demonstrate the effective use of computational techniques for rapid and precise molecular characterisation. The findings encourage innovation in material design and process optimisation in the chemical industry.

ACKNOWLEDGEMENTS

The Department of Applied Sciences and Humanities, Ajay Kumar Garg Engineering College, Ghaziabad, India, and the Department of Physics at Deva Nagri College, Meerut, India, are acknowledged by the authors for their assistance in carrying out this study and completing this investigation.

CONFLICT OF INTERESTS

The authors declare that there is no conflict of interest.

AUTHOR CONTRIBUTIONS

The present work is related to *SDG-9: Industry, Innovation and Infrastructure*. All the authors contributed significantly to this manuscript, participated in reviewing/editing and approved the final draft for publication. The research profile of the authors can be verified from their ORCID ids, given below:

Bandana Sharma https://orcid.org/0000-0002-8401-1254
Munish Kumar Yadav https://orcid.org/0000-0003-1540-9733

Cite this article as: B. Sharma and M. K. Yadav, *Rasayan J. Chem.*, 19(2), 1166-1176(2026), https://doi.org/10.31788/RJC.2026.1929753.

REFERENCES

1. M. Anjalin, N. Kanagathara, A.R. Baby Suganthi, *Materials Today: Proceedings*, **33**, 4751(2020), https://doi.org/10.1016/j.matpr.2020.08.358
2. T. Celestino, *Organics*, **6**, 20(2025), https://doi.org/10.3390/org6020020
3. N. L. John, S. Abraham, D. Sajan , B.K. Sarojini , B. Narayana, *Journal of Molecular Structure*, **1222**, 128939 (2020), https://doi.org/10.1016/j.molstruc.2020.128939
4. A. R. Kumar, S. Selvaraj, P. Anthoniammal, R. J. Ramalingam, B. Ranjith, P. Jayaprakash and G. P. S. Mol, *Journal of Fluorine Chemistry*, **270**, 110167(2023), https://doi.org/10.1016/j.jfluchem.2023.110167
5. K. Haruna, A. A. Alenaizan, Abdulaziz A. Al-Saadi , *RSC Advances*, **6**, 67794(2016), https://doi.org/10.1039/C6RA11908E
6. M. Karnan, V. Balachandran, M. Murugan, *Journal of Molecular Structure*, **1039**, 197(2013), https://doi.org/10.1016/j.molstruc.2013.01.070

7. A. Eşme and S. G. Sağdınç, *Journal of Applied Spectroscopy*, **84**, 1098(2018), https://doi.org/10.1007/s10812-018-0594-8
8. E. Kose, M. Karabacak, A. Atac, *Spectrochimica Acta Part A: Molecular and Biomolecular Spectroscopy*, **143**, 265(2015), https://doi.org/10.1016/j.saa.2015.01.079
9. E. Kose, M. Karabacak, F. Bardak, A. Atac, *Journal of Molecular Structure*, **1123**, 284(2016), https://doi.org/10.1016/j.molstruc.2016.05.088
10. J. Westermayr, P. Marquetand. *Chemical Science,* **16**, 21660(2025), https://doi:10.1039/D5SC05628D
11. H. Ren, H. Li, Q. Zhang, L. Liang, W. Guo, F. Huang, Y. Luo, J. Jiang, *Fundamental Research*, **1**, 488(2021), https://doi.org/10.1016/j.fmre.2021.05.005
12. M. George, N. L. John, M. S. Kumar, A. Subashini, D. Sajan, *Journal of Molecular Structure*, **1128**, 754(2017), https://doi.org/10.1016/j.molstruc.2016.09.034
13. S. Sevvanthi, S. Muthu, M. Raja, S. Aayisha, S. Janani, *Heliyon*, **6**, e04724(2020), https://doi.org/10.1016/j.heliyon.2020.e04724
14. B. Revathi, V. Balachandran, B. Raja, K. Anitha, M. Kavimani, *Journal of Molecular Structure*,**1141**, 81(2017), https://doi.org/10.1016/j.molstruc.2017.03.078
15. K. Carthigayan, S. Xavier, S. Periandy, *Spectrochimica Acta Part A: Molecular and Biomolecular Spectroscopy*,**142**, 350(2015), https://doi.org/10.1016/j.saa.2015.02.035
16. X. Meng-Xia and L. Yuan, *Spectrochimica Acta Part A: Molecular and Biomolecular Spectroscopy*, **58**, 2817(2002), https://doi.org/10.1016/S1386-1425(02)00072-0
17. S. Kaluva, V. L. Karri, M. Naganathappa, *Optical and Quantum Electronics*, **55**, 874(2023), https://doi.org/10.1007/s11082-023-05132-w
18. A. Jumabaev, B. Khudaykulov, I. Doroshenko, H. Hushvaktov, A. Absanov, *Vibrational Spectroscopy*, **122**, 103422(2022), https://doi.org/10.1016/j.vibspec.2022.103422
19. P. Wojciechowski, K. Helios, D. Michalska, *Vibrational Spectroscopy*, **57**, 126(2011), https://doi.org/10.1016/j.vibspec.2011.06.001
20. Y. Erdogdu, Ş. Yurdakul, S. Badoglu, M.T. Güllüoğlu, *Journal of Molecular Structure*, **1184**, 364(2019), https://doi.org/10.1016/j.molstruc.2019.02.016
21. K. Haruna, T. A. Saleh, J. Al Thagfi, A. A. Al-Saadi, *Journal of Molecular Structure*, **1121**, 7(2016), https://doi.org/10.1016/j.molstruc.2016.05.021
22. V. Mukherjee, Karunakar Singh, N.P. Singh, R.A. Yadav, *Spectrochimica Acta Part A: Molecular and Biomolecular Spectroscopy*, **73**, 44(2009), https://doi.org/10.1016/j.saa.2009.01.024
23. V. Mukherjee, N.P. Singh, R.A. Yadav, *Spectrochimica Acta Part A: Molecular and Biomolecular Spectroscopy*, **73**, 249(2009), https://doi.org/10.1016/j.saa.2009.02.014
24. A. Usha Rani, N. Sundaraganesan, M. Kurt, M. Cinar, M. Karabacak, *Spectrochimica Acta Part A: Molecular and Biomolecular Spectroscopy*, **75**, 1523(2010), https://doi.org/10.1016/j.saa.2010.02.010
25. M. Arivazhagan, D. A. Rexalin, *Spectrochimica Acta Part A: Molecular and Biomolecular Spectroscopy*, **96**, 668(2012), https://doi.org/10.1016/j.saa.2012.07.040
26. M. Karabacak, Z. Calisir, M. Kurt, E. Kose, A. Atac, *Spectrochimica Acta Part A: Molecular and Biomolecular Spectroscopy*, **153**, 754(2016), https://doi.org/10.1016/j.saa.2015.09.007
27. A. R. Kumar, L. Ilavarasan, G.P. Sheeja Mol, S. Selvaraj, Mohammad Azam, P. Jayaprakash, M. Kesavan, Mahboob Alam, J. Dhanalakshmi, Saud I. Al-Resayes, A. Ravi, *Journal of Molecular Structure*, **1298**, 136974(2024), https://doi.org/10.1016/j.molstruc.2023.136974
28. V. Karunakaran, V. Balachandran, *Spectrochimica Acta Part A: Molecular and Biomolecular Spectroscopy*, **98**, 229(2012), https://doi.org/10.1016/j.saa.2012.08.003
29. C. S. Abraham, J. C. Prasana, S. Muthu, *Spectrochimica Acta Part A: Molecular and Biomolecular Spectroscopy*, **181**, 153(2017), https://doi.org/10.1016/j.saa.2017.03.045
30. C. S. Abraham, J. C. Prasana, S. Muthu, F. Rizwana B, M. Raja, *Journal of Molecular Structure*, **1160**, 393(2018), https://doi.org/10.1016/j.molstruc.2018.02.022

[RJC-9753/2026]